


## Article

# Improvement of Quantitative Single-Photon Emission Computed Tomography Image Quality by the New Step-and-Shoot Scan Mode

Hiroki Yamamoto <sup>1,2,\*</sup>, Ami Sasaki <sup>3</sup>, Mizuki Osaka <sup>3</sup>, Koji Shirakawa <sup>2</sup>, Morio Seino <sup>2</sup>, Takaaki Matsuhashi <sup>2</sup>, Yasuyuki Takahashi <sup>1</sup>, Tsutomu Zeniya <sup>4</sup> , Shota Hosokawa <sup>1</sup>, Masataka Narita <sup>2</sup> and Masahiko Aoki <sup>5</sup>

- <sup>1</sup> Department of Radiation Science, Graduate School of Health Sciences, Hirosaki University, 66-1 Hon-cho, Hirosaki 036-8564, Aomori, Japan; ytaka3@hirosaki-u.ac.jp (Y.T.); shosokawa@hirosaki-u.ac.jp (S.H.)
- <sup>2</sup> Department of Radiology, Division of Medical Technology, Hirosaki University Hospital, 53 Hon-cho, Hirosaki 036-8563, Aomori, Japan; shirakawa\_ko@hirosaki-u.ac.jp (K.S.); ms0225@hirosaki-u.ac.jp (M.S.); tmatsuhashi@hirosaki-u.ac.jp (T.M.); nari-hiroin@hirosaki-u.ac.jp (M.N.)
- <sup>3</sup> Department of Radiation Technology, School of Health Sciences, Hirosaki University, 66-1 Hon-cho, Hirosaki 036-8564, Aomori, Japan; h18m2218@hirosaki-u.ac.jp (A.S.); h18m2203@hirosaki-u.ac.jp (M.O.)
- <sup>4</sup> Graduate School of Science and Technology, Hirosaki University, 3 Bunkyo-cho, Hirosaki 036-8561, Aomori, Japan; zeniya@hirosaki-u.ac.jp
- <sup>5</sup> Department of Radiation Oncology, Graduate School of Medicine, Hirosaki University, 5 Zaifu-cho, Hirosaki 036-8562, Aomori, Japan; maoki@hirosaki-u.ac.jp
- \* Correspondence: hyamamoto@hirosaki-u.ac.jp; Tel.: +81-172-33-5111



**Citation:** Yamamoto, H.; Sasaki, A.; Osaka, M.; Shirakawa, K.; Seino, M.; Matsuhashi, T.; Takahashi, Y.; Zeniya, T.; Hosokawa, S.; Narita, M.; et al.

Improvement of Quantitative Single-Photon Emission Computed Tomography Image Quality by the New Step-and-Shoot Scan Mode. *Radiation* **2022**, *2*, 168–176. <https://doi.org/10.3390/radiation2020012>

Academic Editor: Giorgio Treglia

Received: 2 February 2022

Accepted: 3 April 2022

Published: 6 April 2022

**Publisher's Note:** MDPI stays neutral with regard to jurisdictional claims in published maps and institutional affiliations.



**Copyright:** © 2022 by the authors. Licensee MDPI, Basel, Switzerland. This article is an open access article distributed under the terms and conditions of the Creative Commons Attribution (CC BY) license (<https://creativecommons.org/licenses/by/4.0/>).

**Simple Summary:** We compared the image quality of the new single-photon emission computed tomography (SPECT) scan mode (step-and-shoot plus continuous mode) with that of the conventional SPECT scan mode (step-and-shoot mode) in a phantom study and a clinical case study. The effects of various quantitative correction methods on scatter, attenuation, and resolution recovery were also examined in this new scan mode. Accordingly, this new scan mode shortens the scan time and reduces the injected dose because its sensitivity is superior to that of the step-and-shoot mode.

**Abstract:** The step-and-shoot (SS) mode and continuous mode are currently used for single-photon emission computed tomography (SPECT) scan mode, and a new scan mode that combines both modes, step-and-shoot plus continuous (SSC) mode, was developed. It is expected to allow a shorter scan time and lower injected dose because the SSC mode is more sensitive than the SS mode. We confirmed the image quality of this scan mode, including various quantitative correction methods for scatter (SC), attenuation (AC), and resolution recovery (RR) in a phantom study and clinical case study. Image quality was evaluated by the count, contrast-to-noise ratio (CNR), and percent of the coefficient of variation (%CV). Independent of the correction methods, the count, CNR, and %CV of the SSC mode were superior to those of the SS mode. The ACSCRR was the best method, with a maximum increased rate of 66.4% in counts and 57.8% in CNR for the 13-mm sphere and 19.6% in CNR for other sphere sizes. The %CV for the SSC mode was the best for AC and ACRR, which was at 15.1%. With regards to attaining short bone SPECT scan time, the combination of the SSC mode and ACRR or ACSCRR demonstrated the best physical performance.

**Keywords:** step-and-shoot; step-and-shoot plus continuous; Swiftscan; bone SPECT

## 1. Introduction

In bone scintigraphy, whole-body images are mainly acquired, in addition to static images and single-photon emission computed tomography (SPECT) images. Compared with whole-body images alone, the addition of SPECT scan is considered to increase the specificity [1]. However, SPECT scan increases the examination time; thus, if the

examination time for bone scintigraphy is 30 min, the SPECT scan time should be 15 min or less [2]. Therefore, a faster and more sensitive scan mode is needed.

The step-and-shoot (SS) mode and continuous mode have been used as SPECT scan modes. In the SS mode, the detector moves and rests at a certain projection angle and collects  $\gamma$ -rays when the detector is stationary, while the continuous mode allows the collection of data while the detector is rotating at a constant speed. A new step-and-shoot plus continuous (SSC) mode, which is a combination of both SPECT scan modes, has been introduced. This system (NM/CT 860, GE Healthcare, Milwaukee, WI, USA) combines the SSC mode with a new low-energy high-resolution sensitivity collimator (LEHRS) and is marketed as Swiftscan SPECT. It is expected to reduce scan time and the injected dose because increasing projection counts improves sensitivity. Although physical image quality has been evaluated by phantom studies using Swiftscan SPECT and SS mode [3,4], the effects of the scan time and various image correction methods have not been fully investigated.

In this study, we examined the physical performance of the SSC mode with various image correction methods, assuming a short scan time for bone SPECT after whole-body imaging.

## 2. Materials and Methods

### 2.1. Phantom Study

We used the National Electrical Manufacturer Association International Electrical Commission (NEMA IEC) body phantom (AcroBio). Hot spheres with diameters of 37, 28, 22, 17, 13, and 10 mm were placed inside the phantom. The background (BG) region of the NEMA IEC body phantom was filled with 18 kBq/mL of  $^{99m}\text{Tc}$ , and the radioactivity ratio of the BG to the hot spheres was 1:6 [5].

### 2.2. SPECT/CT Image Acquisition and Reconstruction

The SPECT/CT system was a dual-head NM/CT 860 (GE Healthcare) equipped with the LEHRS collimator. The image processor was Xeleris 4DR (GE Healthcare). The image analysis software was Q.Volumetrix MI (GE Healthcare). The region of interest (ROI) and voxel of interest (VOI) Analysis Tool (RAVAT) ver.1.0 (Nihon Medi-Physics) was used for image analysis.

SPECT scans were performed in the SS and SSC modes. The acquisition protocols were a 360° proximity orbit, zoom of 1.0 $\times$ , and matrix size of 128  $\times$  128 (4.42 mm/pixel). The SPECT scan time was set at 3.5 min (sampling angle of 6°, 7 s/view), assuming a 2-step SPECT scan time of approximately 10 min, including the CT scan time. The photo-peak and scatter windows of the SPECT scan were set to 140.5 keV  $\pm$  10% and 120 keV  $\pm$  5%. The CT scan protocols were as follows: tube voltage, 120 kV; tube current, auto mA; noise index, 25; rotation time, 0.98 s; and pitch, 1.675.

SPECT images were reconstructed by ordered-subset expectation maximization (OS-EM) methods (10 subsets, 6 iterations [6]) with the dual-energy window scatter correction (SC), CT attenuation correction (AC), and resolution recovery (RR). A Butterworth filter (cutoff, 0.48 cycles/cm; power factor, 10) was used as a post-processing filter. Four combinations of correction methods were used: OS-EM with AC (AC); OS-EM with AC and SC (ACSC); OS-EM with AC and RR (ACRR); and OS-EM with AC, SC, and RR (ACSCRR).

### 2.3. Phantom Study Data Analyses

#### 2.3.1. Count Rate

Using RAVAT 1.0 image analysis software, a circular ROI was drawn on each hot sphere and BG region of the slice where the 10-mm sphere was most clearly visible [5,7,8]. The ROI size of each hot sphere was set to 70% of its size, and the BG region was placed with 12 circular ROIs of 26 mm diameter on the edge of the phantom (Figure 1). The counts

per pixel in the ROI of each hot sphere and BG were calculated. The increased rate in counts for the SSC mode relative to the SS mode was calculated using Equation (1).

$$\text{Increased rate of count}_i = \frac{C_{SSC,i} - C_{SS,i}}{C_{SS,i}} \times 100 \quad (1)$$

where  $i$  is each hot sphere diameter or BG and  $C_{SSC,i}$  and  $C_{SS,i}$  are the mean counts per pixel in the ROI of each hot sphere or BG region of SPECT images collected in the SS and SSC modes.

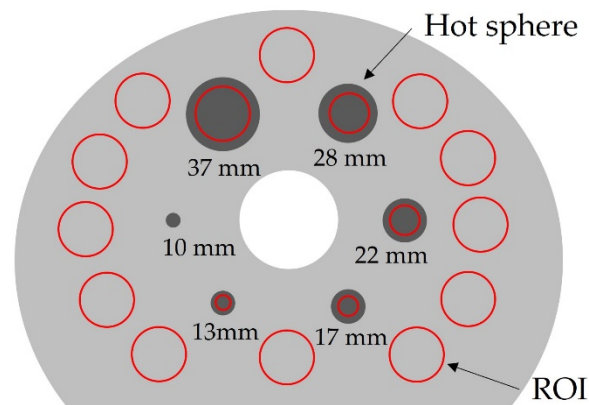


**Figure 1.** Circular region of interest setting for each hot sphere and background region in the NEMA IEC body phantom.

### 2.3.2. CNR

As in Section 2.3.1, circular ROIs were drawn on BG and each hot sphere, and the mean count and standard deviation (SD) per pixel in the ROI were calculated. The CNR was calculated from Equation (2) to evaluate the rendering ability of the hot sphere. In addition, the increase rate of CNR for the SSC mode relative to the SS mode was calculated from Equation (3).

$$\text{CNR}_i = \frac{C_i - C_{BG}}{SD_{BG}} \quad (2)$$

$$\text{Increased rate of CNR}_i = \frac{\text{CNR}_{SSC,i} - \text{CNR}_{SS,i}}{\text{CNR}_{SS,i}} \times 100 \quad (3)$$

where  $C_i$  and  $C_{BG}$  are the mean counts per pixel of the hot sphere and BG,  $SD_{BG}$  is the SD of the BG, and  $\text{CNR}_{SSC,i}$  and  $\text{CNR}_{SS,i}$  are the CNR of each hot sphere in SPECT images scanned in the SS and SSC modes.

### 2.3.3. %CV

To evaluate the BG variability, %CV was calculated from Equation (4), where the slice location and ROI size in BG are the same as in Section 2.3.1.

$$\%CV = \frac{SD_{BG}}{C_{BG}} \times 100 \quad (4)$$

## 2.4. Clinical Case

One patient underwent bone SPECT in the SS and SSC modes 5 h after the intravenous injection of 1000 MBq of  $^{99m}\text{Tc}$ -MDP. One 15-mm diameter circular ROI was set in the tumor region, and five 15-mm diameter circular ROIs were set in the normal bone region of the target location in SPECT images. The CNR and increased CNR rate for each scan mode and image correction methods were calculated and compared using Equations (2) and (3). The acquisition and image reconstruction protocols were used similar to that in the phantom study.

### 3. Results

#### 3.1. Phantom Study

##### 3.1.1. Count Rate

Figure 2 shows the measurements of the mean counts per pixel of the BG and each hot sphere for each scan mode and quantitative correction method, and Table 1 shows the increased rate of counts for the SSC mode in comparison with the SS mode. The counts of BG and all hot spheres increased in the SSC mode compared with the SS mode. Regardless of the scan mode, the counts decreased as the hot sphere diameter became smaller. The 13-mm sphere demonstrated the highest increased rate of counts, and of all the correction methods, the ACSCRR exhibited the highest increased rate of counts.

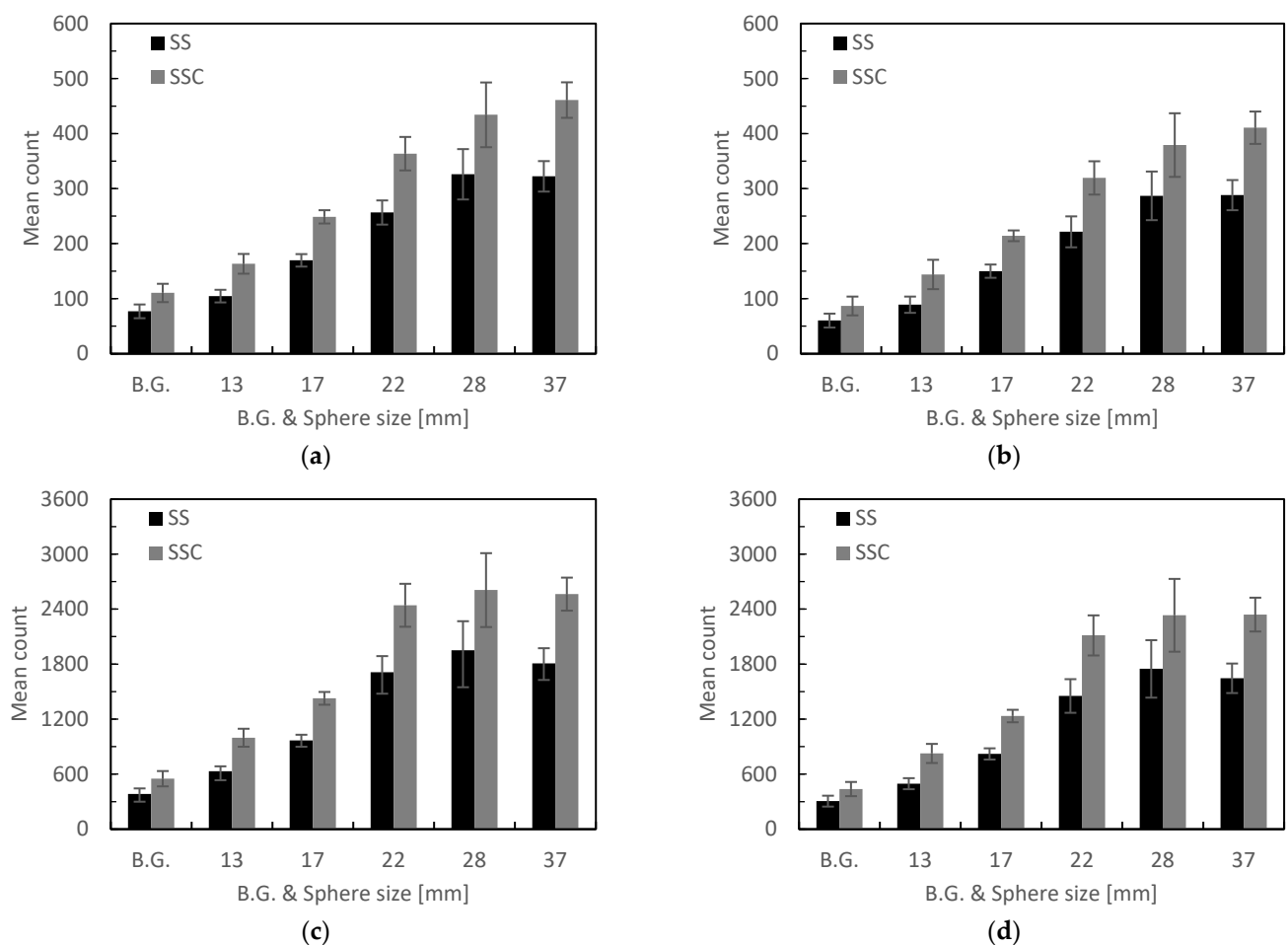


**Figure 2.** Mean counts per pixel of the background region and each hot sphere for scan modes and quantitative correction methods: (a) AC, (b) ACSC, (c) ACRR, and (d) ACSCRR.

**Table 1.** Increased rate of counts for the SSC mode in comparison with the SS mode.

Correction Methods	BG	Sphere Size [mm]				
		13	17	22	28	37
AC	43.7	56.1	46.5	41.6	33.2	43.0
ACSC	43.8	61.8	42.8	44.2	32.2	42.6
ACRR	44.0	57.8	47.5	42.6	33.7	41.8
ACSCRR	43.0	66.4	50.4	45.5	33.4	42.2

(unit: %)

### 3.1.2. CNR

Figure 3 shows the relationship between the CNR and the hot sphere size for the scan modes and collection methods, and Table 2 shows the increased rate of the CNR for the SSC mode compared with the SS mode. The CNR for the SSC mode was higher than that for the SS mode, except for the 28-mm sphere. The increased rate of the CNR was the highest at the 13-mm sphere, and the ACSCRR had a higher increased rate of the CNR than other combinations of correction methods. However, the absolute errors of the CNR between the SS and SSC modes did not change significantly regardless of sphere sizes and correction methods (Table 3).

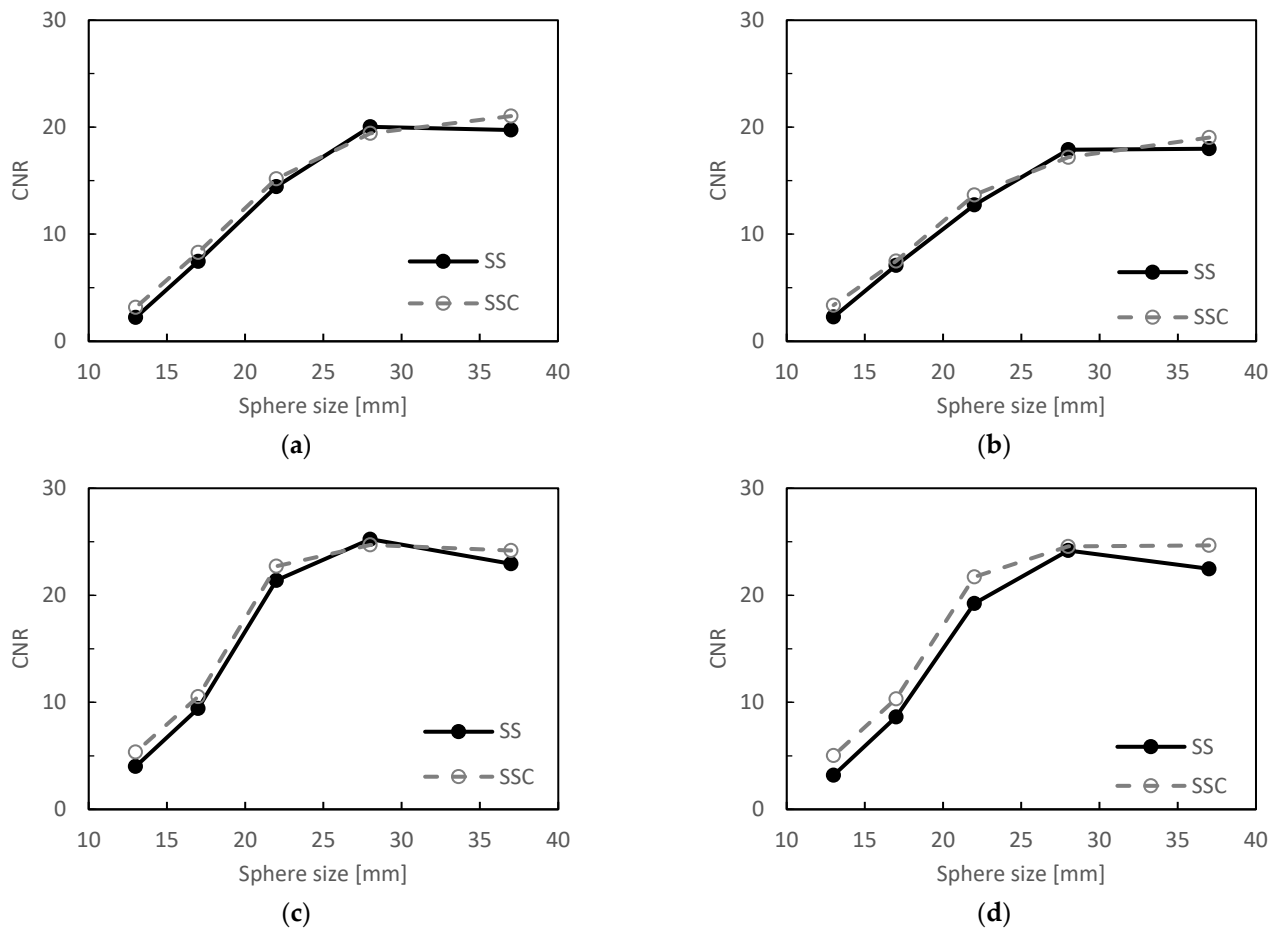


**Figure 3.** Relationship between CNR and hot sphere size for scan modes and correction methods: (a) AC, (b) ACSC, (c) ACRR, and (d) ACSCRR.

**Table 2.** Increased rate of the CNR for the SSC mode compared with the SS mode.

Correction Methods	Sphere Size [mm]				
	13	17	22	28	37
AC	42.1	11.1	5.1	−3.0	6.6
ACSC	48.3	5.7	7.3	−4.0	5.8
ACRR	33.7	11.8	6.2	−2.1	5.4
ACSCRR	57.8	19.6	12.9	1.5	9.8

(unit: %)

**Table 3.** Comparison of absolute error of the CNR between the SS and SSC modes.

Correction Methods	Sphere Size [mm]				
	13	17	22	28	37
AC	0.9	0.8	0.7	0.6	1.3
ACSC	1.1	0.4	0.9	0.7	1.0
ACRR	1.4	1.1	1.3	0.5	1.2
ACSCRR	1.8	1.7	2.5	0.4	2.2

### 3.1.3. %CV

Figure 4 shows the relationship between %CV and correction methods among scan modes. The %CV for the SSC mode was lower than that for the SS mode for all correction methods. In addition, the %CV for the combination of the SSC mode with AC and ACRR was the best among all conditions.

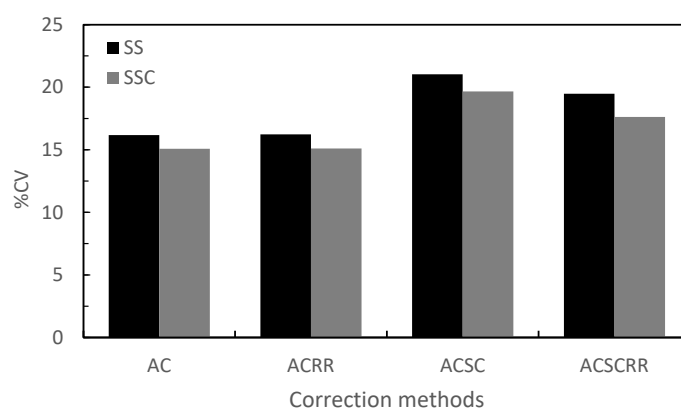
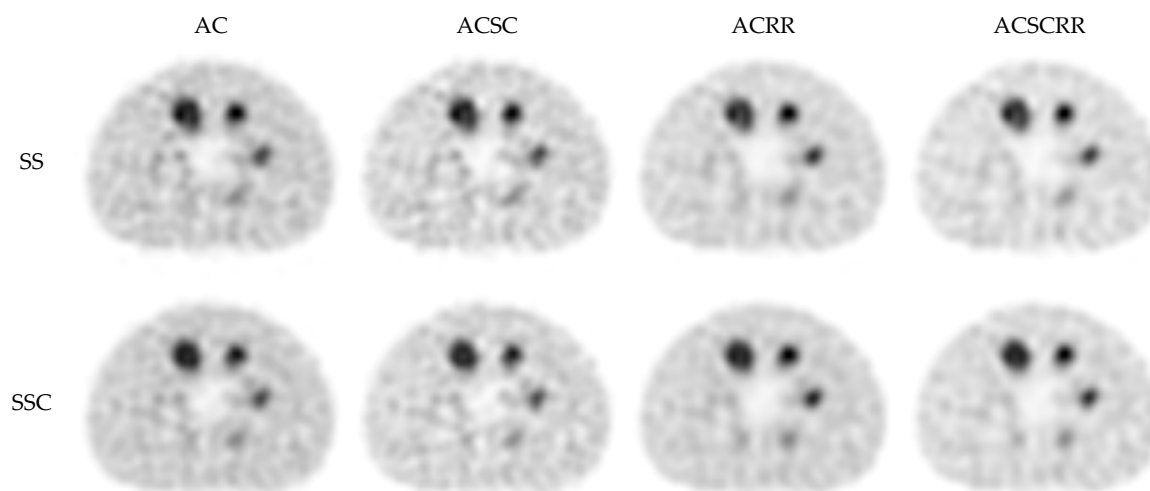
**Figure 4.** Relationship between %CV and correction methods among scan modes.

Figure 5 shows the phantom images for the combination of scan modes and correction methods. The distortion of the hot sphere was observed as the hot sphere diameter became smaller. A low count region was found inside the 37-mm sphere for the SS mode and all correction methods. The 13-mm sphere was visible in the combination of the SSC mode with ACRR and ACSCRR.

**Figure 5.** Phantom images for the combination of scan modes and correction methods. The upper and lower window levels were set to 100% and 0%, respectively.

### 3.2. Clinical Case

Table 4 shows the mean counts, SD, and CNR results in the ROI of the tumor and normal bone regions, and Figure 6 shows the bone SPECT images for each condition. The counts of both tumor and normal bone were increased in the SSC mode. No difference was found in CNR for both scan modes and without RR. With RR, the CNR was slightly increased, and with ACSCRR, the CNR for the SSC mode increased by 10%. The SPECT images reconstructed by the ACRR and ACSCRR demonstrated less noise variation and more contrast than the others.

**Table 4.** Count, SD, and CNR results in a clinical case.

Scan Mode	Correction Methods	Tumor		Normal Bone		CNR
		Mean Count	SD	Mean Count	SD	
SS	AC	122.3	16.7	48.4	7.0	10.6
	ACSC	102.1	17.4	33.7	6.7	10.3
	ACRR	774.9	89.5	275.0	45.7	10.9
	ACSCRR	701.4	88.5	227.6	43.2	11.0
SSC	AC	178.6	19.4	73.3	10.0	10.5
	ACSC	153.9	18.4	54.2	9.7	10.2
	ACRR	1146.4	120.6	409.6	65.8	11.2
	ACSCRR	1038.4	129.6	337.9	58.1	12.1

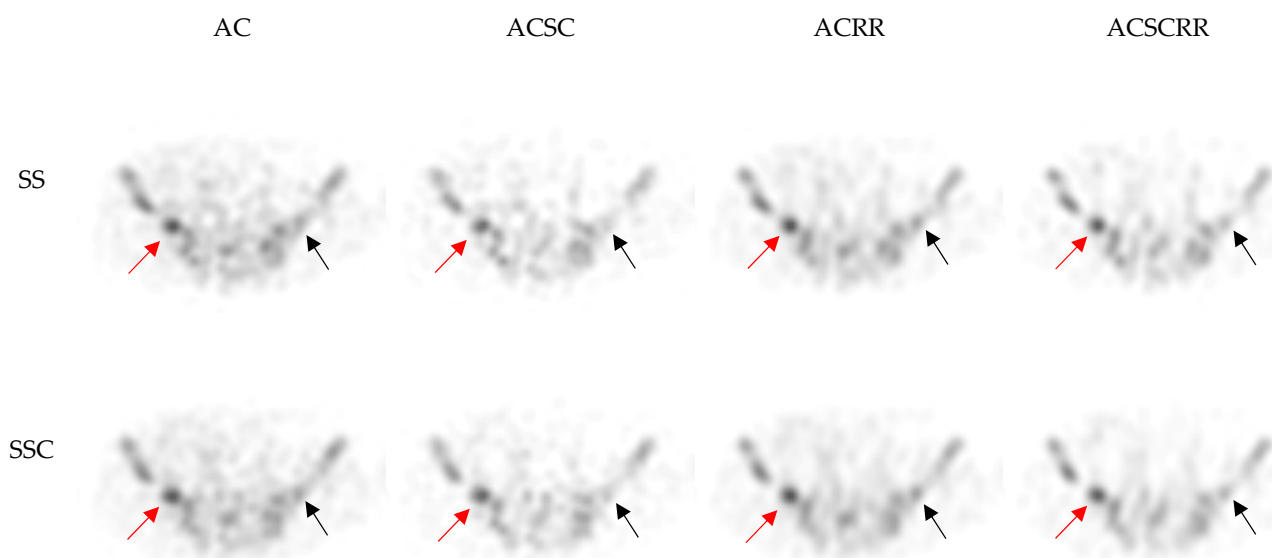


**Figure 6.** Bone SPECT image for each scan mode and correction methods. The upper and lower window levels were set to 30% and 0%, respectively. The red and black arrows represent the tumor and normal bone regions, respectively.

### 4. Discussion

The SSC mode combines the SS mode with the continuous mode. It is expected to shorten the scan time and reduce the injected dose because the sensitivity is increased by collecting data even when the detector is moving. A previous study assessed the usefulness of the Swiftscan SPECT in bone scintigraphy. Swiftscan SPECT has been reported to reduce image noise and improve CNR compared with the SS mode [4]. However, the study was performed only with ACSCRR, and there is no study on the effect of the SSC mode on the image quality by combining other correction methods for SPECT images. In this study, we confirmed the physical performance of the SSC mode, including various quantitative



correction methods for SC, AC, and RR, in a phantom study and a clinical case, assuming a short bone SPECT scan time.

The mean counts per pixel of the BG and hot sphere by the SSC mode were higher than those by the SS mode for all combinations of correction methods, increasing by 32.2–66.4%. However, the CNR for the SSC mode did not increase as much as the count in all hot spheres except for the 13-mm sphere, regardless of correction methods. This is probably because no difference was found in the increased rate of counts between the hot sphere and BG, and the SD of BG for the SSC mode was approximately 30% higher than that for the SS mode. Even if the CNR of the 13-mm sphere was improved by 1–2, the increased rate of CNR was higher because the CNR of the 13-mm sphere was as low as 3–5. For all scan modes and correction methods, the count and CNR were smaller for smaller hot sphere diameters, which is thought to be due to the underestimation by the partial volume effect [9]. The results on the improvement of %CV and CNR for the SSC mode were similar to those reported by Shibutani et al., despite the difference in the phantom used [4].

In the phantom study and clinical cases, counts differed significantly with and without RR, regardless of the correction method. This is due to the RR correction of Q.Volumetrix MI. Although the correction process is not clearly disclosed, the difference in counts was caused by RR correction that increased four times the counts of the projection data.

RR provides better results for CNR and %CV because it increases the spatial resolution and reduces noise [10,11]. In short SPECT scan times, ACSCRR had the highest increased rate of counts and CNR, while the combination of the SSC mode with AC and ACRR had the best %CV. The results of the physical evaluation indicate that the combination of the SSC mode with ACSCRR has better contrast but worse BG variability than that with ACRR. By combining the SSC mode with ACRR and ACSCRR, the 13-mm sphere was visibly confirmed (Figure 5). However, the distortion of the hot sphere was observed as the hot sphere diameter became smaller, regardless of the scan modes and correction methods. In addition, a low count region inside the 37-mm sphere was observed when it was scanned by the SS mode. The SSC mode improved the low count region inside the 37-mm sphere because the counts increased by 32.2–66.4%, but it could not improve the distortion of the hot sphere. Therefore, AC and RR are essential because SC decreases the count because of its principle, or it is important to increase the count of projection data, such as extending the scan time.

Thus, it is necessary to optimize the scan time because the image quality will be degraded at low projection counts regardless of correction methods, even if it is scanned by the SSC mode. The number of iterations and subsets is related to the noise. Especially since clinical images contain numerous noises, increasing the number of iterations and subsets degraded the image quality [12,13]. In the present study, the images were evaluated under clinical conditions (10 iterations, 6 subsets). However, it is necessary to examine how changes in the number of iterations and subsets affect the images in short acquisition times.

In clinical cases, no significant difference was found in the increased rate of counts between the correction methods, with 46.0–50.7% and 48.5–60.8% in the tumor region and normal bone region, respectively, similar to the phantom study. Moreover, the CNR of the SS and SSC modes were different from those of the phantom study, and only the CNR for ACRR and ACSCRR was improved (ACRR 2.8%, ACSCRR 10.0%). The combination of the SSC mode with ACRR and ACSCRR suggests the possibility of a shorter bone SPECT scan time than conventional SS methods. However, since the clinical analysis was based on only one case, it is necessary to increase the number of cases.

## 5. Conclusions

The physical performance of the SS and SSC modes was confirmed using phantoms, including the effect of correction methods and assuming a short bone SPECT scan time. The SSC mode was superior to the SS mode in terms of count, CNR, and %CV, independent of the correction methods. The combination of the SSC mode with ACRR or ACSCRR appears to best detect small lesions within a short SPECT scan time. However, when the projection



count was reduced, the hot sphere could be distorted, which could not be improved by the SSC mode or changing the combination of correction methods. Therefore, the scan time needs to be carefully examined.

**Author Contributions:** Conceptualization, H.Y. and Y.T.; methodology, H.Y.; investigation, H.Y.; writing—original draft preparation, H.Y.; writing—review and editing, A.S., M.O., K.S., M.S., T.M., Y.T., T.Z., S.H., M.N. and M.A.; supervision, Y.T.; project administration, H.Y. All authors have read and agreed to the published version of the manuscript.

**Funding:** This research received no external funding.

**Institutional Review Board Statement:** The study was conducted according to the guidelines of the Declaration of Helsinki and approved by the Institutional Review Board (or Ethics Committee) of Hiroaki University Graduate School of Health Sciences (no. 2019-007, approved on 17 May 2019).

**Informed Consent Statement:** This study used anonymized data. The explanation and consent of the study were posted on the information board.

**Data Availability Statement:** The data presented in this study are available in this article.

**Conflicts of Interest:** The authors declare no conflict of interest.

## References

1. Yang, H.L.; Liu, T.; Wang, X.M.; Xu, Y.; Deng, S.M. Diagnosis of bone metastases: A meta-analysis comparing  $^{18}\text{F}$ FDG PET, CT, MRI and bone scintigraphy. *Eur. Radiol.* **2011**, *21*, 2604–2617. [[CrossRef](#)] [[PubMed](#)]
2. Masuda, Y.; Nagaki, A.; Kawabuchi, Y.; Nobuyoshi, O.; Katafuchi, T.; Teraoka, S.; Yanagisawa, M.; Niida, H.; Hayashi, M. Point of acquisition, processing, display and output for standardized images with clinical usefulness. *Jpn. J. Nucl. Med. Technol.* **2008**, *28*, 13–74.
3. Thibault, F.; Bailly, M.; Le Rouzic, G.; Mettard, G. Clinical evaluation of General Electric new Swiftscan solution in bone scintigraphy on NaI-camera: A head to head comparison with Siemens Symbia. *PLoS ONE* **2019**, *14*, e0222490. [[CrossRef](#)] [[PubMed](#)]
4. Shibutani, T.; Onoguchi, M.; Naoi, Y.; Yoneyama, H.; Konishi, T.; Tatami, R.; Nakajima, K. The usefulness of SwiftScan technology for bone scintigraphy using a novel anthropomorphic phantom. *Sci. Rep.* **2021**, *11*, 2644. [[CrossRef](#)] [[PubMed](#)]
5. Japanese Society of Nuclear Medicine Technology (JSNMT); SPECT Standardization Committee. Guidelines of standardization of bone SPECT imaging. *Jpn. J. Nucl. Med. Technol.* **2017**, *37*, 517–530.
6. Takahashi, Y.; Murase, K.; Mochizuki, T.; Higashino, H.; Yoshifumi, S.; Akiyoshi, K. Evaluation of the number of SPECT projections in the ordered subsets-expectation maximization image reconstruction method. *Ann. Nucl. Med.* **2003**, *17*, 525–530. [[CrossRef](#)] [[PubMed](#)]
7. Nakamura, Y.; Kangai, Y.; Abe, T.; Nakahara, Y. Improvement of Standardized Uptake Value Accuracy in the  $^{99\text{m}}\text{Tc}$  Body SPECT and SPECT/CT: Optimization of the Phantom for Calculating Becquerel Calibration Factor and Correction Method. *Jpn. J. Radiol. Technol.* **2021**, *77*, 921–931. [[CrossRef](#)] [[PubMed](#)]
8. Hayashi, N.; Tokorodani, R.; Kenda, S.; Ogasawara, D.; Yabe, F.; Ito, K. Determination of Bone SPECT Image Reconstruction Conditions in the Head and Neck Region. *Jpn. J. Radiol. Technol.* **2021**, *77*, 700–709. [[CrossRef](#)] [[PubMed](#)]
9. Maeda, Y.; Nagaki, A.; Komi, Y.; Abe, N.; Kashimura, S. Evaluation of resolution correction in single photon emission computed tomography reconstruction method using a body phantom: Study of three different models. *Jpn. J. Radiol. Technol.* **2015**, *71*, 1070–1079. [[CrossRef](#)] [[PubMed](#)]
10. Takahashi, Y.; Murase, K.; Mochizuki, T.; Sugawara, Y.; Maeda, H.; Kinda, A. Simultaneous 3-dimensional resolution correction in SPECT reconstruction with an ordered-subsets expectation maximization algorithm. *J. Nucl. Med. Technol.* **2007**, *35*, 34–38. [[PubMed](#)]
11. Onishi, H.; Motomura, N.; Fujino, K.; Natsume, T.; Haramoto, Y. Quantitative performance of advanced resolution recovery strategies on SPECT images: Evaluation with use of digital phantom models. *Radiol. Phys. Technol.* **2013**, *6*, 42–53. [[CrossRef](#)] [[PubMed](#)]
12. Ogawa, K. Image reconstruction by ordered subsets expectation maximization method. *Jpn. J. Med. Phys.* **1999**, *19*, 184–192.
13. Shigenori, M.; Masamichi, Y. Basic evaluation of OSEM algorithm by assessing iteration times and number of subsets in a hot spot phantom study. *Jpn. J. Radiol. Technol.* **2001**, *57*, 1233–1239. [[CrossRef](#)]